Journal of Materials Chemistry A

Improved Performance by Morphology Control via Fullerenes in PBDT-TBT-alkoBT based Organic Solar Cells

Journal:	*Journal of Materials Chemistry A*
Manuscript ID:	TA-ART-04-2015-002709.R1
Article Type:	Paper
Date Submitted by the Author:	21-May-2015

Complete List of Authors:	Khatiwada, Devendra; South Dakota State University, Electrical Engineering Qiao, Qiquan; South Dakota State university, Electrical Engineering Venkatesan, Swami; SDSU, Electrical Engineering Chen, Qiliang; South Dakota State University, Center for Advanced Photovoltaics Chen, Jihua; Oak Ridge National Laboratory, Center for Nanophase Materials Sciences Dubey, Ashish; SDSU, Electrical Engineering Adhekari, Nirmal; South Dakota State university, Electrical Engineering Mitul, Abu; South Dakota State University, Center for Advanced Photovoltaics Mohammad, Lal; South Dakota State University, Center for Advanced Photovoltaics

Improved Performance by Morphology Control via Fullerenes in PBDT-TBT-alkoBT based Organic Solar Cells

Devendra Khatiwada[1], Qiliang Chen[1], Swaminathan Venkatesan[1], Jihua Chen[2], Nirmal Adhikari [1], Ashish Dubey[1], Abu Farzan Mitul[1], Lal Mohammed[1] and Qiquan Qiao[1]*

[1]Center for Advanced Photovoltaics, Department of Electrical Engineering and Computer Science, South Dakota State University, Brookings, SD, USA
qiquan.qiao@sdstate.edu

[2]Center for Nanophase Materials Sciences, Oak Ridge National Laboratory, Oak Ridge, TN 37831, USA

Abstract

In this work, we report improved performance by controlling morphology using different fullerene derivatives in poly{2-octyldodecyloxy-benzo[1,2-b;3,4-b]dithiophene-alt-5,6-bis(dodecyloxy)-4,7- di(thieno[3,2-b]thiophen-2-yl)-benzo[c][1,2,5]thiadiazole} (PBDT-TBT-alkoBT) based organic solar cells. $PC_{60}BM$ and $PC_{70}BM$ fullerenes were used to investigate the characteristic change in morphology and device performance. Fullerene affects device efficiency by changing active layer morphology. $PC_{70}BM$ with broader absorption than $PC_{60}BM$ resulted in reduced device performance which was elucidated by the intermixed granular morphology separating each larger grain in the $PC_{70}BM$/polymer composite layer which created higher density of traps. However after adding additive 1,8-diiodooctane (DIO), the fibrous morphology was observed due to reduced solubility of polymer and increased solubility of $PC_{70}BM$ in chloroform. The fibrous morphology improved charge transport leading to increase in overall device performance. Atomic force microscopies (AFM), photo induced charge extraction by linearly increasing voltage (photo-CELIV), and Kelvin prove force microscope (KPFM) were used to investigate nanoscale morphology of active layer with different fullerene derivatives. For $PC_{60}BM$ based active layer, AFM images revealed dense fibrous morphology and more distinct fibrous morphology was observed by adding DIO. The $PC_{70}BM$ based active layer only exhibited intermixed granular morphology instead of fibrous morphology observed in $PC_{60}BM$ based active layer. However, addition of DIO in $PC_{70}BM$ based active layer led to fibrous morphology. When additive DIO was not used, a wider distribution of surface potential was observed for $PC_{70}BM$ than $PC_{60}BM$ based active layer by KPFM measurements, indicating

polymer and fullerene domains are separated. When DIO was used, narrower distribution of surface potential for both $PC_{70}BM$ and $PC_{60}BM$ based active layers was observed. Photo-CELIV experiment showed larger extracted charge carrier density and mobility in $PC_{70}BM$/DIO film.

Keywords: Fullerene, morphology, additive, organic solar cell

Introduction

Inexpensive fabrication, low temperature processing, mechanical flexibility and light weight have made organic photovoltaic device a promising candidate for future solar cells [1-5]. Bulk heterojunction (BHJ) structure has widely been used with insight of achieving high efficiency solar cells up to 10% consisting of intermixed donor and acceptor network of conjugated polymer and fullerenes[6]. For high efficient polymer solar cells, electrochemical properties and energy levels of fullerene acceptor are very important. Fullerene derivative $PC_{60}BM$ or $PC_{70}BM$ as an acceptor is extensively used in bulk heterojunction solar cell [7-9]. The energy levels of fullerene derivative acceptor can be changed by using bisadducts and multiadducts PCBM consist of two or more functional groups. The LUMO level of those fullerene was found to be higher than normal PCBM, thus increasing open circuit V_{oc}. However, symmetric property of fullerene derivative PCBM was disturbed in bisadduct and multiadduct fullerenes hindering electron transport[10]. Thus, these excellent fullerene derivatives exhibiting high performance in the polymer fullerene composite has always been limited [11]. The energy level of fullerene derivative and its electrochemical properties in ternary blend system containing fullerenes $PC_{61}BM$/ $PC_{71}BM$ mixture with polymer shows enhanced power conversion efficiency (PCEs) due to enhanced absorption of $PC_{71}BM$ and balanced charge transport of $PC_{61}BM$ [12]. In addition, the chemical structure of fullerenes [13], its miscibility in polymer [14] , intercalation [15], position of C_{60} in some regioisomer (bisadduct) fullerenes helps to tune the device performance [16, 17].

To optimize BHJ morphology several parameters such as choice of solvent [18], condition of the film casting [19], post-film deposition technique, effect of additive [20], temperature, concentration, treatment for electron and hole transport layer [21], deposition of electrode have been taken under consideration. These parameters are directly affected due to presence of fullerene derivatives. Fullerene derivatives have thus become ubiquitous acceptors because of their high electron affinity, ability to transport charge effectively and tune morphology.

However, the impact of fullerene derivatives on morphology and optoelectronic properties of polymer has not been explained.

In this paper we investigated the changes in morphology of novel polymer PBDT-TBT-alkoBT due to addition of fullerene derivatives $PC_{60}BM$ and $PC_{70}BM$ respectively. In addition optoelectronic properties of novel polymer PBDT-TBT-alkoBT intermixed with fullerenes $PC_{60}BM$ and $PC_{70}BM$ were studied. Atomic force microscopy (AFM), photo induced charge extraction by linearly increasing voltage (CELIV), and Kelvin prove force microscope (KPFM) were used to correlate nanoscale morphology of polymer with different fullerene derivatives.

Experimental section

The alternating copolymer PBDT-TBT-alkoBT (C-107) was prepared by a typical Suzuki polymerization in the lab. Phenyl-C61/C70 butyric acid methyl ester ($PC_{60}BM$) and $PC_{70}BM$ were ordered from Nano-C. Zinc acetate dehydrate, ethanolamine, 1,8-diiodooctane (DIO), MoO_3, Ag and 2-methoxyethanol were purchased from Sigma Aldrich. 1 mg of zinc acetate dehydrate [$Zn(CH_3COOH.2H_2O)$] dissolved in 2-methoxyethanol (CH_3OCH_2OH, 10 ml) and 0.28 mg of mono-ethanolamine ($NH_2CH_2CH_2OH$) as stabilizer was used to prepare Zinc oxide sol-gel. The solution was vigorously stirred for 12 hr.

For device fabrication, indium tin oxide (ITO) coated glass slides were cleaned by ultra-sonication for 20 min in detergent water, de-ionized water, acetone and 2-propanol sequentially followed by oxygen plasma cleaning for 25 min before spin-coating a sol-gel ZnO layer. ZnO sol-gel was coated at 4500 rpm for 1 min and then kept on a hot plate at 60 °C for 5 min to remove residual solvent and finally annealed at 200 °C for 30 min. ZnO coated substrates were then transferred to nitrogen filled glove box having lower than 1 ppm of O_2 and H_2O. DIO additive was added with concentration of 2% and 4% by volume 10 min before spin coating. The blend solution PBDT-TBT-alkoBT: PCBM (1:2) with additive was spin-coated at 600 rpm for 60 sec and then transferred to a thermal evaporator where 10 nm of molybdenum trioxide (MoO_3) and 80 nm of silver (Ag) were thermally evaporated in vacuum below $2x10^{-6}$ Torr.

Current density - voltage characteristic measurements were performed on Agilent 4155C semiconductor parameter analyzer. Xenon arc lamp was used as light source (AM 1.5). Silicon photo detector was used as standard which was calibrated from National Renewable Energy

laboratory (NREL). Device was fabricated using ITO substrate (1.5 cm × 1.5 cm) having a cell area of 0.16 cm^2. External quantum efficiency (EQE) measurements were done using Xenon lamp attached to a Newport monochromator.

Agilent 8453 spectrophotometer was used to determine UV-vis absorption. Blank scan was first performed on ZnO coated ITO substrates followed by sample scan of active layer. Atomic force microscopy was used to determine the topography image [22]. AFM was conducted in tapping mode using Agilent 5500 SPM (scanning probe microscope). Tips of AFM were made with silicon, coated with Cr/Pt having a resonance frequency of ~300 KHz. Kelvin prove force microscopy (KPFM) was performed in a single pass AM-FM mode giving information on topography and surface potential. Topography was done in AM mode and KPFM was done in FM mode. Gwyddion software was used to analyze the AFM and KPFM images.

Energy filtered transmission electron microscopy (EFTEM) was performed with Zeiss Libra 120 kV. PEDOT:PSS coated substrates were immersed in deionized water. Active layer floated on the surface of water was picked with 600 mesh honey comb shaped Ni grids (Ted Pella). Information on domain composition was given by EFTEM which generated elemental map of polymer and fullerene [23, 24]. EFTEM images were taken in 19eV ± 5eV for donor map (donor brighter) and 30eV± 5eV for acceptor map (acceptor brighter). Selective area electron diffraction (SAED) experiment was performed in the transmission electron microscope (TEM) [25, 26]. SAED pattern was recorded with 576 mm camera length. Al (111) was used as calibration standard (0.234 nm).

Photo-induced current extraction by linear increasing voltage (Photo-CELIV) technique was used to determine recombination lifetime, extracted charge carrier density and charge carrier mobility (μ) [27, 28]. Experiment was designed in our lab using a nanosecond laser (OBB OL-401), a function generator and a digital oscilloscope integrated together, operated using a customized Lab-view program. Keeping solar cell in open circuit condition, a laser pulse was incident on the device. After certain varying delay time, a voltage ramp was given for extracting photo-generated charge carriers.

Electrochemical cyclic voltammetry measurement was conducted to determine the highest occupied molecular orbitals (HOMOs) and lowest unoccupied molecular orbitals

(LUMOs) of the polymer [29, 30]. The apparatus consists of a carbon rod as working electrode, Ag/AgCl as reference electrode and platinum wire as counter electrode. Voltage was swept at a scan rate of 50 mV/s at room temperature. Ferrocene was used as an external reference. 0.1 M of tetra butyl ammonium phosphorus hexafluoride ($TBAPF_6$) in anhydrous acetonitrile (CH_3CN) solution was used as electrolyte. First the oxidation onset of ferrocene was obtained from calculation. A thin layer of C-107 was coated on carbon electrode for the HOMO and LUMO measurements.

Results and discussion

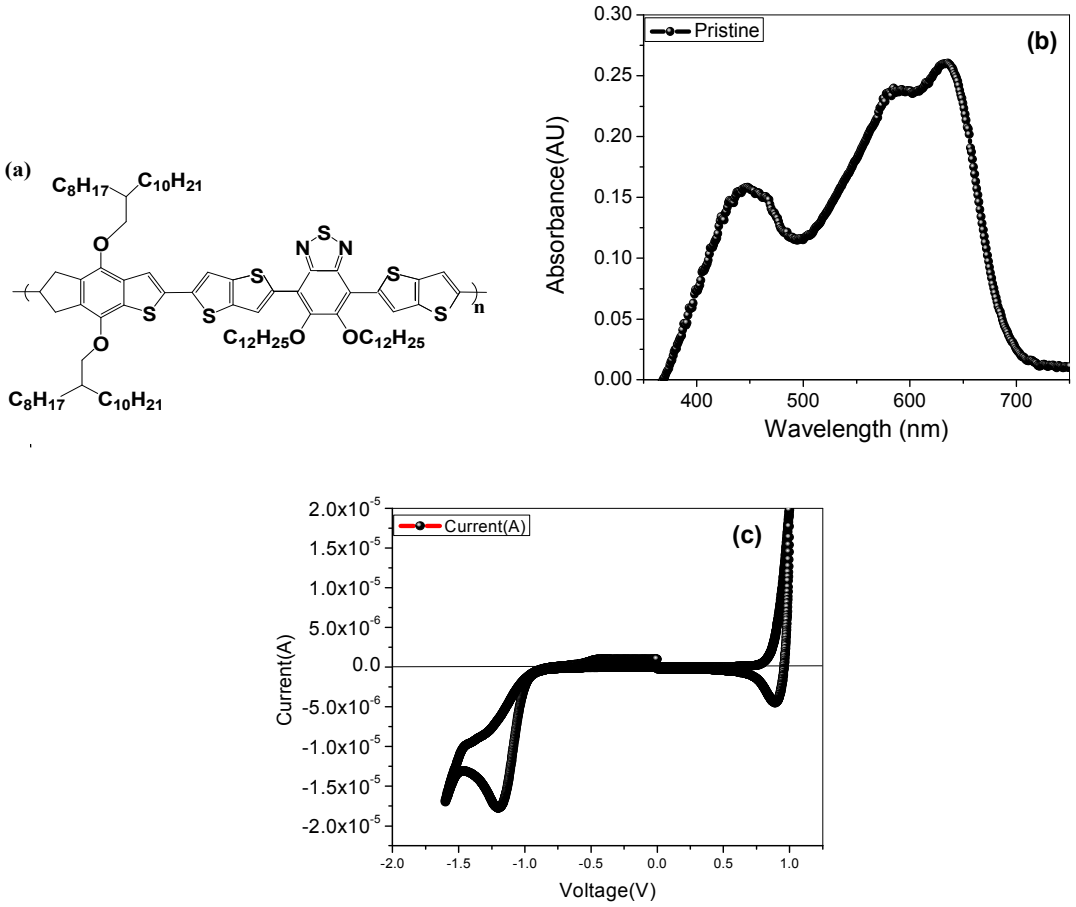

Figure 1. (a) Molecular structure, (b) absorbance spectrum, and (c) cyclic voltammetry of PBDT-TBT-alkoBT thin films.

Chemical structure of co-polymer PBDT-TBT-alkoBT is shown in Figure 1 (a). UV-vis absorbance spectrum of pure polymer is as shown in Figure 1 (b). The absorption peak at 650 nm is pronounced for pure polymer. Pure polymer has two observed peaks due to the donor (BDT)

and acceptor (TBT) unit at 450 nm and 650 nm respectively. The optical bandgap measured by the absorption onset (λ = 710 nm) is ~ 1.74 eV. Cyclic voltammetry was used to determine the highest occupied molecular orbital (HOMO) and lowest unoccupied molecular orbital (LUMO). The HOMO and LUMO levels of the polymer were found to be about -5.65 eV and -3.85 eV respectively, leading to an electrochemical band gap of ~1.80 eV.

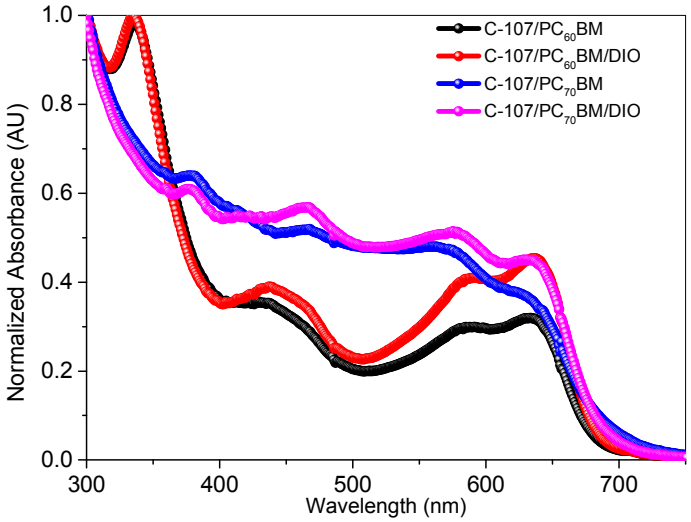

Figure 2. Absorbance spectra of PBDT-TBT-alkoBT (C-107) films with (a) $PC_{60}BM$, (b) $PC_{60}BM$/DIO, (c) $PC_{70}BM$, and (d) $PC_{70}BM$/DIO.

Figure 2 shows absorbance spectra of polymer:$PC_{60}BM$ and $PC_{70}BM$ with and without DIO. The peak observed at 350 nm is due to fullerene absorption and those at 450 nm and 600 nm correspond to the absorption of polymer. Absorption at 450 nm caused by polymer donor unit is more pronounced for film casted with $PC_{70}BM$ and $PC_{70}BM$/DIO due to broad absorption of fullerene $PC_{70}BM$ in the visible spectrum. The intensity of vibronic peak is found to increase with addition of DIO which characterizes molecular ordering in the blend film. Literature reveals that the higher structural order is induced by poor solubility of fullerene in DIO [31, 32].

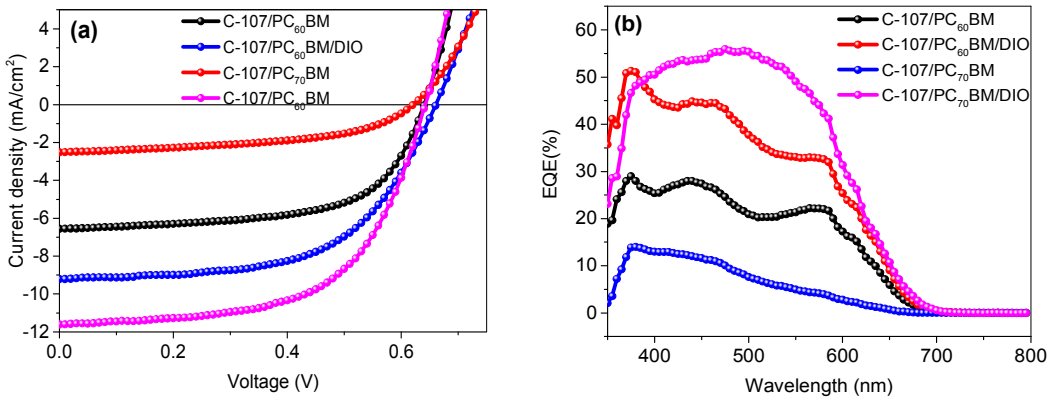

Figure 3. (a) Current density vs voltage (J-V) characteristics and (b) external quantum efficiency (EQE) for solar cells from PBDT-TBT-alkoBT(C-107) with $PC_{60}BM$, $PC_{60}BM$/DIO, $PC_{70}BM$, and $PC_{70}BM$/DIO.

Table 1. Photovoltaic performance from cells with $PC_{60}BM$ and $PC_{70}BM$ fullerenes with series and shunt resistance.

	V_{oc} (V)	J_{sc} (mA/cm^2)	FF	Efficiency (%)	Shunt Resistance	Series Resistance
C-107/ $PC_{60}BM$	0.64	6.55	0.62	2.59	1762.11	32.95
C-107/ $PC_{70}BM$	0.62	2.51	0.50	0.78	1023.803	79.91
C-107/ $PC_{60}BM$/DIO	0.66	9.21	0.57	3.52	526.31	26.32
C-107/ $PC_{70}BM$/DIO	0.64	11.60	0.59	4.42	649.08	17.92

Figure 3 shows Current density vs voltage (J-V) curves and EQE of solar cells from $PC_{60}BM$ and $PC_{70}BM$ with and without the addition of DIO. Short circuit current density (J_{sc}) increased from 6.50 mA/cm^2 to 7.5 mA/cm^2 for $PC_{60}BM$ and from 2.52 mA/cm^2 to 11.6 mA/cm^2 for $PC_{70}BM$ with addition of DIO which led to enhancement in power conversion efficiency. Results are summarized in table1. External quantum efficiency (EQE) without additive is lower than that with additive (DIO) added to the solution within the entire wavelength region. In spite of increase in absorption intensity with $PC_{70}BM$ fullerene, EQE is found to decrease indicating significant difference in molecular interaction.

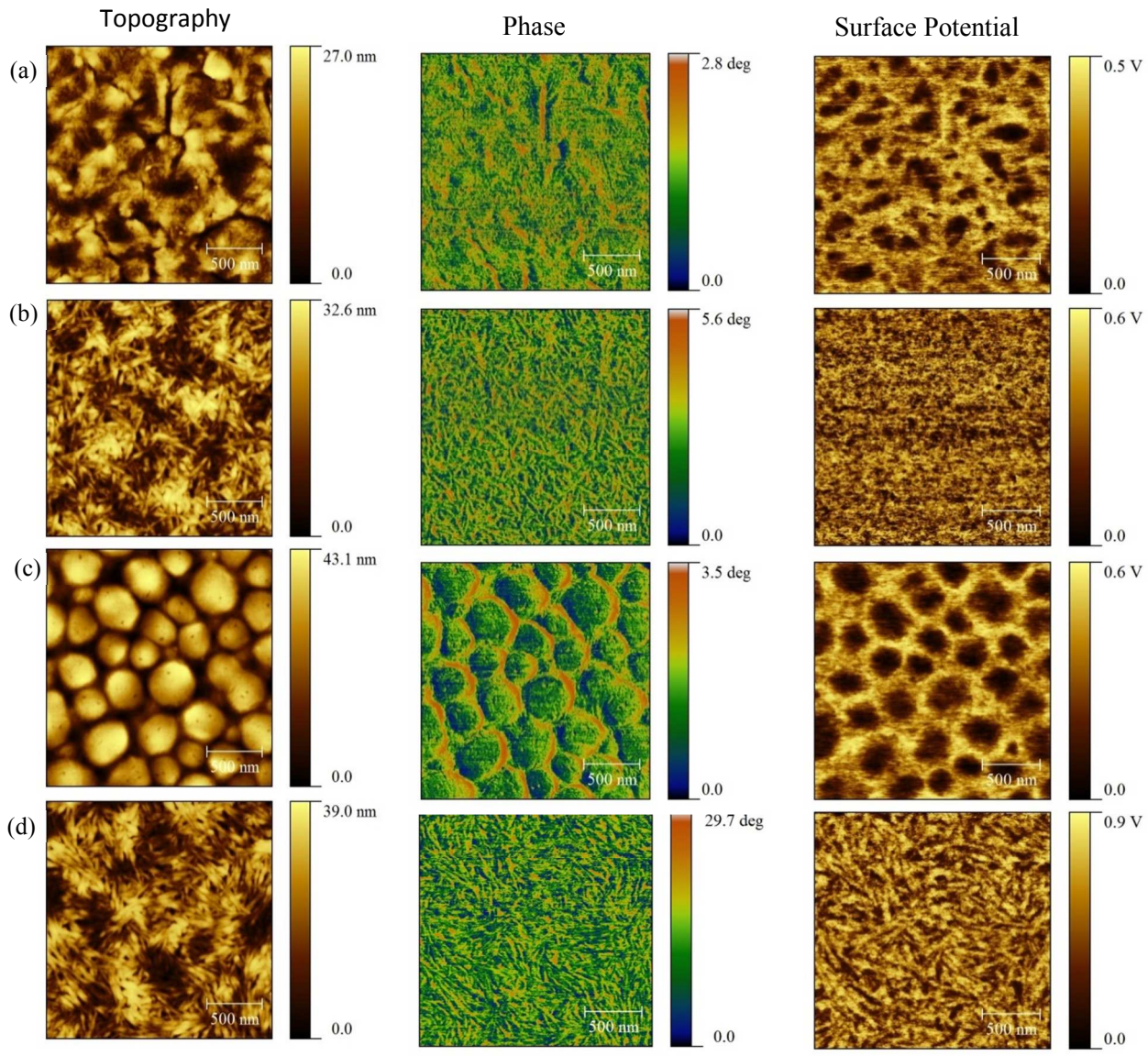

Figure 4. Atomic force microscopy (AFM) topography, phase and surface potential images of PBDT-TBT-alkoBT (C-107) with (a) $PC_{60}BM$, (b) $PC_{60}BM$/DIO, (c) $PC_{70}BM$, and (d)) $PC_{70}BM$/DIO (scale represents 500 nm)

In order to investigate the surface morphology, atomic force microscope (AFM) measurement was carried out with and without solvent additive for polymer $PC_{60}BM$ and $PC_{70}BM$ respectively. AFM images for blends with $PC_{60}BM$ and $PC_{70}BM$ are as shown in figure 4. Topography images show that films processed with DIO as additive have more fibrous surface

morphology as DIO leads to the aggregation of polymer phase into crystalline fibers. The RMS roughness for blend films with $PC_{60}BM$, $PC_{60}BM$/DIO, $PC_{70}BM$, and $PC_{70}BM$/DIO is 3.05 nm, 3.75 nm, 8.49 nm and 3.38 nm, respectively. The $PC_{70}BM$ blend film exhibits much rougher surface showing aggregation of polymer and fullerene. The phase images show different color contrast that indicates an intermixed phase. Big granular morphology was observed in the $PC_{70}BM$ based blend. These spherical domains are separated from each other with larger interface gap.

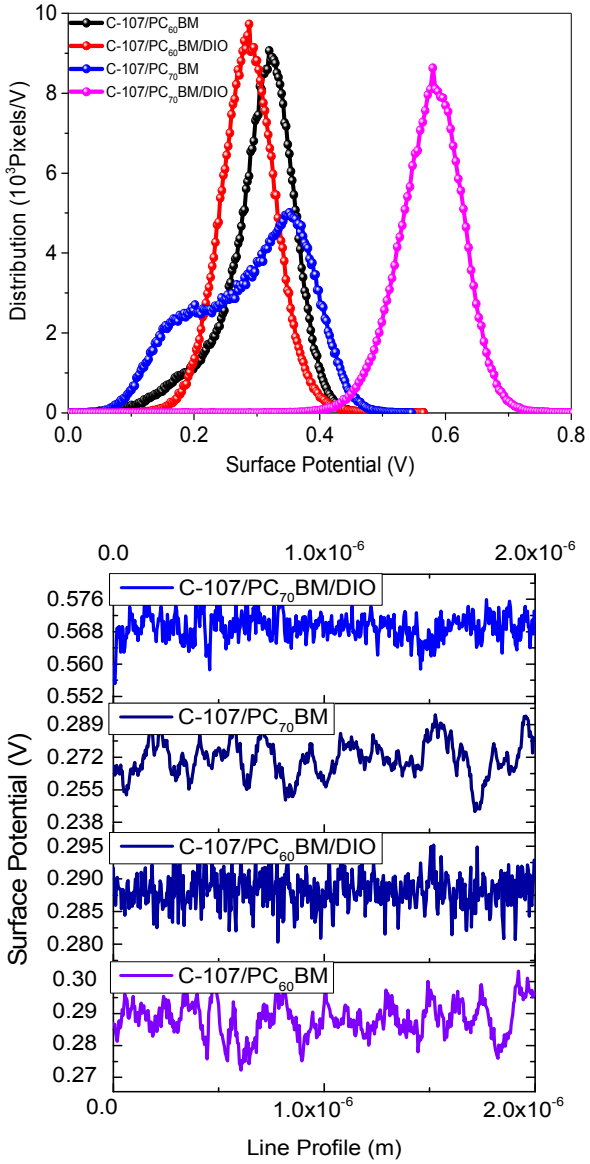

Figure 5 (a) Surface potential distribution and (b) line profile distribution of PBDT-TBT-alkoBT (C-107) with $PC_{60}BM$, $PC_{60}BM$/DIO, $PC_{70}BM$ and $PC_{70}BM$/DIO.

Kelvin probe microscope (KPFM) was used to measure local surface potential. As shown in Figure 5a, the $PC_{60}BM$:polymer composite shows a narrower potential distribution with higher surface potential value than $PC_{70}BM$ based mixture. When DIO was added, the work function of $PC_{60}BM$:polymer composite decreased. The $PC_{70}BM$:polymer composite exhibits a wider distribution of potential with one shoulder and one peak. Polymer distribution is illustrated with sharp peak while that of fullerene by the shoulder. However, when DIO is added to $PC_{70}BM$:polymer composite, the surface potential gets higher with a narrower distribution potential. For the films fabricated with additive, line profile in figure 5b shows finer variation of surface potential which indicates finer phase separation whereas for the films fabricated without additive shows least variation of surface potential [33].

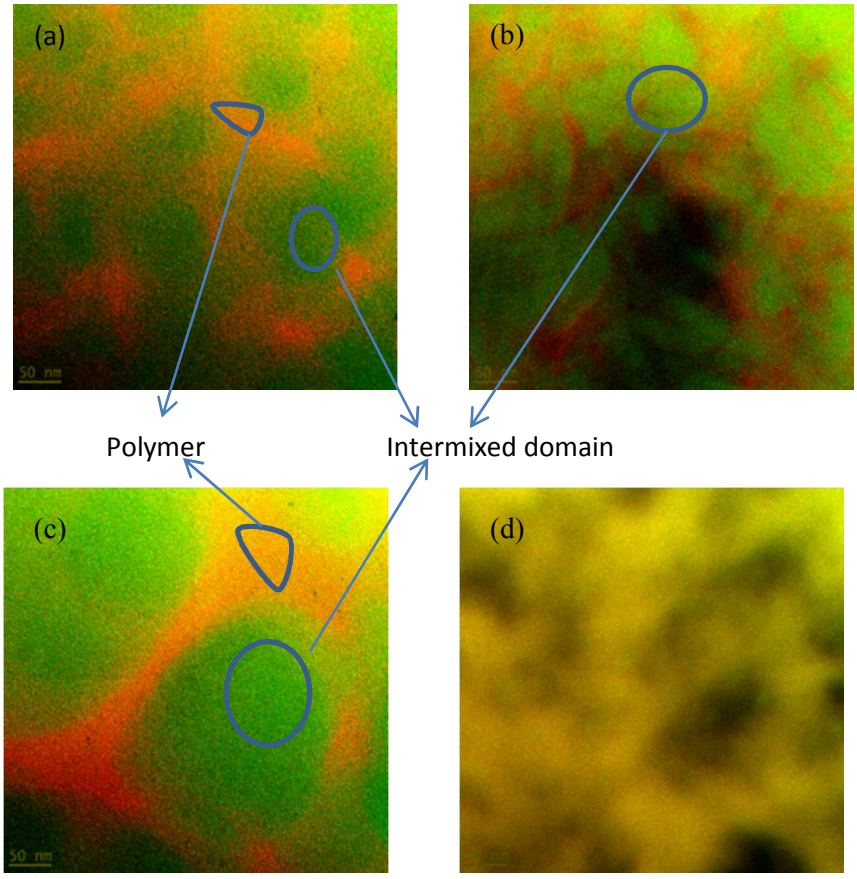

Figure 6. Energy filtered transmission electron microscope (EFTEM) images of PBDT-TBT-alkoBT (C-107) with (a) $PC_{60}BM$, (b) $PC_{60}BM$/DIO, (c) $PC_{70}BM$ and (d) $PC_{70}BM$/DIO.

Figure 6 (a), (b) (c) and (d) shows EFTEM image of polymer PBDT-TBT-alkoBT with fullerenes $PC_{60}BM$, $PC_{70}BM$, $PC_{60}BM$/DIO and $PC_{70}BM$/DIO, respectively. EFTEM Images shows intermixed domain surrounded by polymer boundary except with film fabricated with fullerene $PC_{70}BM$/DIO. Donor and acceptor map (supporting information) shows contrasts inversion indicating intermixed domain. However, the film fabricated with $PC_{70}BM$/DIO does not show contrast inversion and both the donor and acceptor map images are mirror image of each other, due to the large thickness variation in sample film. Polymer forms a skin layer thus leading to vertical charge transport more prominent. This is due to fullerene $PC_{70}BM$ being more soluble in solvent (chloroform) with DIO. Thus, DIO remains in solution and is more soluble to fullerene leading aggregation of polymer resulting to nanoscale phase separation.

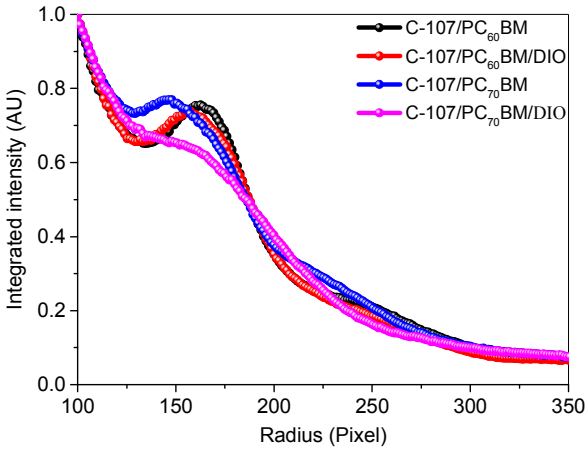

Figure 7. Radial profile distribution of PBDT-TBT-alkoBT (C-107) with $PC_{60}BM$, $PC_{70}BM$, $PC_{60}BM$/DIO and $PC_{70}BM$/DIO.

Figure 7 shows radial profile distribution of polymer:$PC_{60}BM$ and $PC_{70}BM$ with and without DIO obtained from selected area electron diffraction (SAED) pattern. The peak at the 150 pixel is attributed to the d spacing of polymer. Prominent peak is observed in all cases except $PC_{70}BM$/DIO that exhibits higher solubility of fullerene $PC_{70}BM$ in solvent (chloroform) with DIO.

Charge carrier mobility (average of electron and hole mobilities) of the blend was calculated using photo-charge carrier extraction by linear increasing voltage (Photo-CELIV) technique. The equation used is

$$\mu = \frac{2d^2}{3At_{max}^2\left[1 + 0.36\frac{\Delta j}{j_0}\right]}$$

Where, ΔJ is the extraction current maximum, A is voltage ramp speed, J_0 is the capacitive displacement current, d is the thickness of the active layer and t_{max} is the time to reach this maximum extraction current. The Photo-CELIV curve at 7μs delay time for film with $PC_{60}BM$ and $PC_{70}BM$ as fullerene is as shown in Figure 8a. The extracted charge carrier vs delay time plot is shown in Figure 8b. Before the application of voltage ramp, the extracted charge carrier density decreases with increase in delay time for all the devices. The extracted charge carrier density for $PC_{70}BM$/DIO film increases by four orders of magnitude as compared to $PC_{70}BM$ films. The enhanced extracted charge carrier density and mobility in $PC_{70}BM$/DIO solar cells is highest attributing to the effect of fullerene and DIO in finer phase seperation.

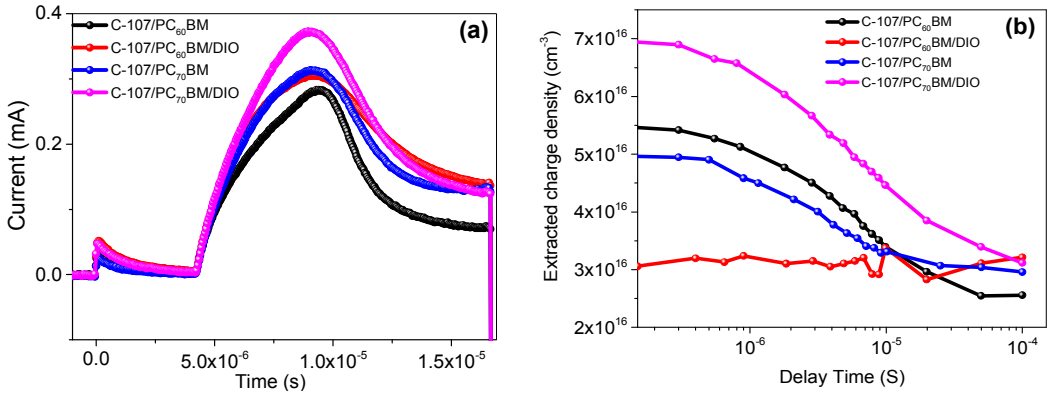

Figure 8. (a) Photo-CELIV spectra (b) extracted charge carrier density versus delay time of PBDT-TBT-alkoBT (C-107) with $PC_{60}BM$, $PC_{60}BM$/DIO, $PC_{70}BM$ and $PC_{70}BM$/DIO at 7μs delay time between light pulse and applied voltage ramp.

Table 2. Charge carrier mobility (μ), time to extract maximum charge carriers (t_{max}), extracted charge carrier density (n_{ext}). Values were estimated from photo-CELIV measurements.

	Charge carrier mobility (μ, $m^2V^{-1}S^{-1}$)	time to extract maximum charge carriers (t_{max}, μs)	Extracted charge carrier density (n, cm^{-3})
$PC_{60}BM$	1.099×10^{-9}	5.55	4.27×10^{16}
$PC_{60}BM$/DIO	1.93×10^{-9}	5.30	3.60×10^{16}
$PC_{70}BM$	1.71×10^{-9}	5.25	3.54×10^{16}
$PC_{70}BM$/DIO	1.58×10^{-9}	5.10	5.33×10^{16}

Conclusions

Inverted structure bulk heterojunction solar cells were fabricated using two different fullerenes and their effects on active layer morphology was studied. The $PC_{70}BM$ based devices exhibited lower device efficiency than $PC_{60}BM$ due to lower J_{sc}, FF and higher series resistance. This was attributed to larger bimolecular recombination and granular active layer morphology with grains separated by larger interface. Addition of DIO leads to increase in overall efficiency by finer phase separation between fullerene and polymer. The $PC_{70}BM$: PBDT-TBT-alkoBT composite shows larger bimolecular recombination than fullerene $PC_{60}BM$. The bimolecular recombination decreases with addition of DIO. Solubility of $PC_{70}BM$ is higher in solvent (chloroform) with DIO leading to finer phase separation.

Acknowledgements

This research was benefited from the grants including NASA EPSCoR (NNX13AD31A), NSF CAREER (ECCS-0950731), and NSF MRI (grant no. 1229577). TEM (J.C.) experiments were conducted at the Center for Nanophase Materials Sciences, which is a DOE Office of Science User Facility.

References

1. J. You, L. Dou, Z. Hong, G. Li and Y. Yang, *Prog. Polym. Sci.*, 2013, **38**, 1909-1928.
2. G. Li, R. Zhu and Y. Yang, *Nature Photonics*, 2012, **6**, 153-161.
3. F. C. Krebs, S. A. Gevorgyan and J. Alstrup, *Journal of Materials Chemistry*, 2009, **19**, 5442-5451.
4. H.-Y. Chen, J. Hou, S. Zhang, Y. Liang, G. Yang, Y. Yang, L. Yu, Y. Wu and G. Li, *Nature Photonics*, 2009, **3**, 649-653.
5. C. Deibel and V. Dyakonov, *Rep. Prog. Phys.*, 2010, **73**, 096401.
6. J. D. Chen, C. Cui, Y. Q. Li, L. Zhou, Q. D. Ou, C. Li, Y. Li and J. X. Tang, *Advanced Materials*, 2014.
7. D. Mühlbacher, M. Scharber, M. Morana, Z. Zhu, D. Waller, R. Gaudiana and C. Brabec, *Advanced Materials*, 2006, **18**, 2884-2889.
8. E. Bundgaard and F. C. Krebs, *Solar Energy Materials and Solar Cells*, 2007, **91**, 954-985.
9. C. Winder and N. S. Sariciftci, *Journal of Materials Chemistry*, 2004, **14**, 1077-1086.
10. J. Hou and X. Guo, in *Organic Solar Cells*, Springer, 2013, pp. 17-42.
11. Y. Sun, J. Seifter, M. Wang, L. A. Perez, C. Luo, G. C. Bazan, F. Huang, Y. Cao and A. J. Heeger, *Advanced Energy Materials*, 2014, **4**.
12. S. J. Ko, W. Lee, H. Choi, B. Walker, S. Yum, S. Kim, T. J. Shin, H. Y. Woo and J. Y. Kim, *Advanced Energy Materials*, 2014.
13. E. I. Altman and R. J. Colton, *Surface science*, 1992, **279**, 49-67.
14. D. Khatiwada, S. Venkatesan, J. Chen, Q. Chen, N. Adhikari, A. Dubey, A. F. Mitul, L. Mohammad, J. Sun and C. Zhang, 2015.

15. N. C. Cates, R. Gysel, Z. Beiley, C. E. Miller, M. F. Toney, M. Heeney, I. McCulloch and M. D. McGehee, *Nano letters*, 2009, **9**, 4153-4157.
16. S. Kitaura, K. Kurotobi, M. Sato, Y. Takano, T. Umeyama and H. Imahori, *Chem. Commun.*, 2012, **48**, 8550-8552.
17. N. D. Treat, A. Varotto, C. J. Takacs, N. Batara, M. Al-Hashimi, M. J. Heeney, A. J. Heeger, F. Wudl, C. J. Hawker and M. L. Chabinyc, *Journal of the American Chemical Society*, 2012, **134**, 15869-15879.
18. Y. Yao, J. Hou, Z. Xu, G. Li and Y. Yang, *Advanced Functional Materials*, 2008, **18**, 1783-1789.
19. J. Peet, M. L. Senatore, A. J. Heeger and G. C. Bazan, *Advanced Materials*, 2009, **21**, 1521-1527.
20. J. K. Lee, W. L. Ma, C. J. Brabec, J. Yuen, J. S. Moon, J. Y. Kim, K. Lee, G. C. Bazan and A. J. Heeger, *Journal of the American Chemical Society*, 2008, **130**, 3619-3623.
21. Y. Sun, J. H. Seo, C. J. Takacs, J. Seifter and A. J. Heeger, *Advanced Materials*, 2011, **23**, 1679-1683.
22. D. Khatiwada and S. K. Lamichhane, *Himalayan Physics*, 2011, **2**, 80-83.
23. S. V. Kesava, Z. Fei, A. D. Rimshaw, C. Wang, A. Hexemer, J. B. Asbury, M. Heeney and E. D. Gomez, *Adv. Energy Mater.*, 2014.
24. F. Hofer, W. Grogger, G. Kothleitner and P. Warbichler, *Ultramicroscopy*, 1997, **67**, 83-103.
25. V. D. Mihailetchi, L. J. A. Koster, P. W. Blom, C. Melzer, B. de Boer, J. K. van Duren and R. A. Janssen, *Adv. Funct. Mater.*, 2005, **15**, 795-801.
26. Q. Lu, K. Yao, D. Xi, Z. Liu, X. Luo and Q. Ning, *J. Mater. Sci. Technol*, 2007, **23**, 189.
27. G. Adam, A. Pivrikas, A. M. Ramil, S. Tadesse, T. Yohannes, N. S. Sariciftci and D. A. M. Egbe, *J Mater Chem*, 2011, **21**, 2594-2600.
28. D. A. M. Egbe, G. Adam, A. Pivrikas, A. M. Ramil, E. Birckner, V. Cimrova, H. Hoppe and N. S. Sariciftci, *J Mater Chem*, 2010, **20**, 9726-9734.
29. X. Li and A. R. Barron.
30. L. LEONAT, G. SBÂRCEA and I. V. BRÂNZOI.
31. P. Adhikary, S. Venkatesan, P. P. Maharjan, D. Galipeau and Q. Q. Qiao, *Ieee T Electron Dev*, 2013, **60**, 1763-1768.
32. S. Venkatesan, N. Adhikari, J. Chen, E. C. Ngo, A. Dubey, D. W. Galipeau and Q. Qiao, *Nanoscale*, 2014, **6**, 1011-1019.
33. S. Venkatesan, J. Chen, E. C. Ngo, A. Dubey, D. Khatiwada, C. Zhang and Q. Qiao, *Nano Energy*.

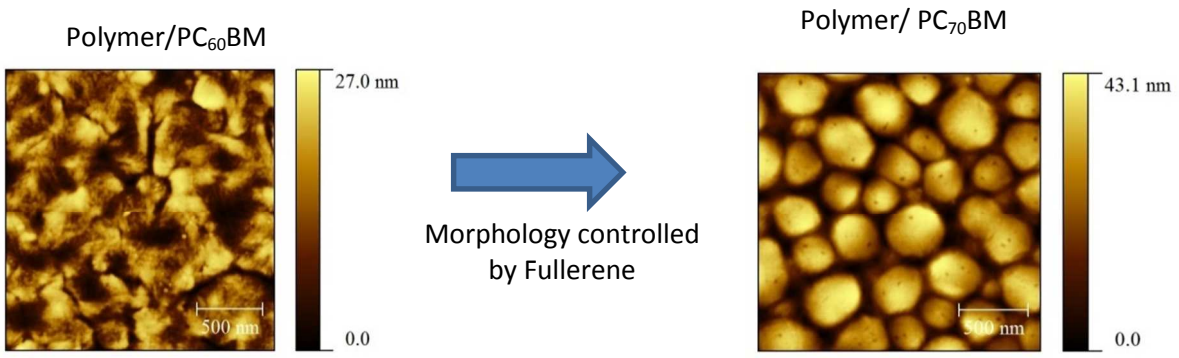
Polymer/PC60BM
27.0 nm
500 nm
0.0
Morphology controlled
by Fullerene
Polymer/ PC70BM
43.1 nm
500 nm
0.0